Solid State Ionics 301 (2017) 99–105

Contents lists available at ScienceDirect

Solid State Ionics

journal homepage: www.elsevier.com/locate/ssi

Conductivity and redox stability of new perovskite oxides $SrFe_{0.7}TM_{0.2}Ti_{0.1}O_{3-\delta}$ (TM = Mn, Fe, Co, Ni, Cu)

Peter I. Cowin [b], Rong Lan [a], Christophe T.G. Petit [b], Dongwei Du [a], Kui Xie [d], Huanting Wang [c], Shanwen Tao [a,c,*]

[a] School of Engineering, University of Warwick, Coventry CV4 7AL, UK
[b] Department of Chemical & Process Engineering, University of Strathclyde, Glasgow G1 1XJ, UK
[c] Department of Chemical Engineering, Monash University, Clayton, Victoria 3800, Australia
[d] Fujian Institute of Research on the Structure of Matter, Chinese Academy of Sciences, Fuzhou, Fujian 350109, China

ARTICLE INFO

Article history:
Received 21 August 2016
Received in revised form 14 January 2017
Accepted 23 January 2017
Available online xxxx

Keywords:
Redox stable
Conductivity
Perovskite
Strontium ferrite
Solid oxide fuel cell

ABSTRACT

New perovskite oxides $SrFe_{0.7}TM_{0.2}Ti_{0.1}O_{3-\delta}$ (TM = Mn, Fe, Co, Ni, Cu) were synthesised by sol-gel processes. Their redox stability and conductivity in both air and 5%H_2/Ar were investigated in details. The cubic perovskite structure was also observed for all dopants with variation in the lattice parameters associated with different dopant environments and charge compensation mechanisms. Improvement of the electronic conductivity over $SrFe_{0.9}Ti_{0.1}O_{3-\delta}$ was observed for all dopants in air, attributed to increasing charge carrier concentrations. Reduction in 5% H_2/Ar exhibited minimal a material properties for $SrFe_{0.7}Cu_{0.2}Ti_{0.1}O_{3-\delta}$, with a significant reduction in conductivity was observed for $SrFe_{0.7}Mn_{0.2}Ti_{0.1}O_{3-\delta}$. All doped compounds exhibited a single phase cubic perovskite structure after reduction in 5%H_2/Ar at 700 °C with the exception of $SrFe_{0.7}Ni_{0.2}Ti_{0.1}O_{3-\delta}$ and $SrFe_{0.7}Co_{0.2}Ti_{0.1}O_{3-\delta}$ which displays secondary nickel and cobalt phases respectively upon reduction. $SrFe_{0.7}Cu_{0.2}Ti_{0.1}O_{3-\delta}$ is redox stable at a temperature below 700 °C and highly conductive with conductivities around 10 S cm^{-1} in both air and reducing atmosphere which are about five times higher than those of pure $SrFe_{0.9}Ti_{0.1}O_{3-\delta}$. In terms of conductivity and redox stability, it is a potential redox stable electrode material for reversible and symmetrical solid oxide fuel cells as well.

1. Introduction

Redox-stable and conductive oxide materials are very useful in application in anode materials for solid oxide fuel cells (SOFCs). Development of redox stable anode for intermediate temperature solid oxide fuel cells (IT-SOFCs) is very important for use as electrode for reversible or symmetric solid oxide fuel cells [1–8]. The electrode materials for reversible and symmetric solid oxide fuel cells must be redox stable or redox reversible. They should exhibit high electrical conductivity in both air and reducing atmosphere [9–12]. In the reported redox stable oxides, $SrFe_{0.75}Mo_{0.25}O_{3-\delta}$ is an excellent material with electrical conductivity of 50 S cm-1 at 850 °C in dry 5 vol% H_2/Ar [13]. This is slightly lower than those reported in the original report for $Sr_2Fe_{1.5}Mo_{0.5}O_{6-\delta}$ [14] although different conductivity values were also reported indicating the conductivity of the materials is very much related to the synthetic history [13]. $SrFeO_{3-\delta}$ based materials are promising electrodes for solid oxide fuel cells. It has been reported that Fe-dope doped $SrTiO_3$ with composition $SrTi_{0.3}Fe_{0.7}O_{3-\delta}$ and $SrTi_{0.6}Fe_{0.4}O_{3-\delta}$ exhibit good anode performance for SOFCs when combined with $Ce_{0.9}Gd_{0.1}O_2$ [15]. Research into B-site doped strontium ferrites has concentrated on stabilisation of the cubic perovskite structure. Doping with cations with a similar oxidation state has also been shown to result in the formation of the cubic perovskite phase for $SrFeO_{3-\delta}$ through suppression of oxygen vacancy ordering [16–18]. This can be achieved through random distribution of dopant cations which either preferentially associate with oxygen vacancies [17] or which repulse oxygen vacancies [18]. Our previous research into titanium doped strontium ferrites, $SrFe_{1-x}Ti_xO_{3-\delta}$ ($x \le 0.3$) indicating $SrFe_{0.9}Ti_{0.1}O_{3-\delta}$ exhibits desired conductivity and redox stability, reduced thermal expansion coefficient compared to $SrFeO_{3-\delta}$, which is a promising redox stable anode for IT-SOFCs [19]. $SrFe_{0.9}Ti_{0.1}O_{3-\delta}$ was also reported as a good cathode for SOFCs [20]. It has been reported that good performance has been achieved when $Sr_{0.98}Fe_{0.8}Ti_{0.2}O_{3-\delta}$ was used as electrode for SOFCs [21]. Cobalt-free perovskite oxide $SrNb_xFe_{1-x}O_{3-\delta}$ was a good cathode for intermediate temperature solid oxide fuel cells (IT-SOFCs) [22]. In our previous study, it was posited that minimal doping of $SrFe_{0.9}Ti_{0.1}O_{3-\delta}$ with cations with a lower oxidation state could be utilised to improve the conductivity whilst retaining the redox stability [19]. To this end a series of transition metal (TM) doped strontium titanium ferrites, $SrFe_{0.7}TM_{0.2}Ti_{0.1}O_{3-\delta}$ (TM = Mn, Fe, Co, Ni, Cu), were synthesised and their stability and

* Corresponding author at: School of Engineering, University of Warwick, Coventry CV4 7AL, UK.
E-mail address: S.Tao.1@warwick.ac.uk (S. Tao).

http://dx.doi.org/10.1016/j.ssi.2017.01.017

conductivity in oxidising and reducing atmospheres elucidated in this paper in order to explore their potential as electrode materials for SOFCs.

2. Experimental

2.1. Synthesis

$SrFe_{0.7}TM_{0.2}Ti_{0.1}O_{3-\delta}$ (TM = Fe, Co, Cu, Mn, Ni) were produced by sol-gel processes. Stoichiometric amounts of $Sr(NO_3)_2$ (98%, Alfa Aesar) and $Fe(NO_3)_3 \cdot 9\ H_2O$ (98%, Alfa Aesar) with either $Co(NO_3)_2 \cdot 6\ H_2O$ (98^{+}%, Alfa Aesar), $Cu(NO_3)_2 \cdot 2.5\ H_2O$ (ACS grade 98–102%, Alfa Aesar), $MnC_4H_6O_4 \cdot 4\ H_2O$ (>99%, Sigma Aldrich) or $Ni(NO_3)_2 \cdot 6\ H_2O$ (98%, Alfa Aesar) were dissolved in distilled water. A stoichiometric amount of titanium isopropoxide ($C_{12}H_{28}O_4Ti$) (97%, Alfa Aesar) was dissolved in ethanol and the solutions were combined, whilst maintaining a 2:1 ratio of ethanol to distilled water. Citric acid (99^{+}%, Alfa Aesar) was added in a 2:1 ratio to metal ions and the solution was heated until gelation. The resultant gel was fired at 600 °C for 2 h. A second firing at 1300 °C for 3 h was then performed. Pellets of all the samples (ø ≈ 13 mm × 2 mm) were uniaxially pressed at 221 MPa and sintered in air at 1300 °C for 2 h.

2.2. Analytical procedures

Phase purity and crystal parameters of the samples were examined by X-ray diffraction (XRD) analysis using a Bruker D8 Advance diffractometer (Cu $K_{\alpha 1}$ radiation, λ = 1.5405 Å). GSAS [23] software was used to perform a least squares refinement of the lattice parameters of all the samples.

The densities of the pellets were determined from the measured mass and volume. Theoretical densities were calculated using experimental lattice parameters and the chemical formula $SrFe_{0.9}Ti_{0.1}O_{3-\delta}$ and $SrFe_{0.7}TM_{0.2}Ti_{0.1}O_{3-\delta}$ (TM = Co, Cu, Mn, Ni). The relative densities were calculated from the actual and theoretical density values. The density of the pellets was 75–85% for all compounds.

Thermal analysis was conducted using a Stanton Redcroft STA 1500 Thermal Analyser between room temperature and 800 °C with a heating/cooling rate of 10 °C min^{-1} in either air or 5% H_2/Ar with gas flow rates of 50 mL min^{-1}.

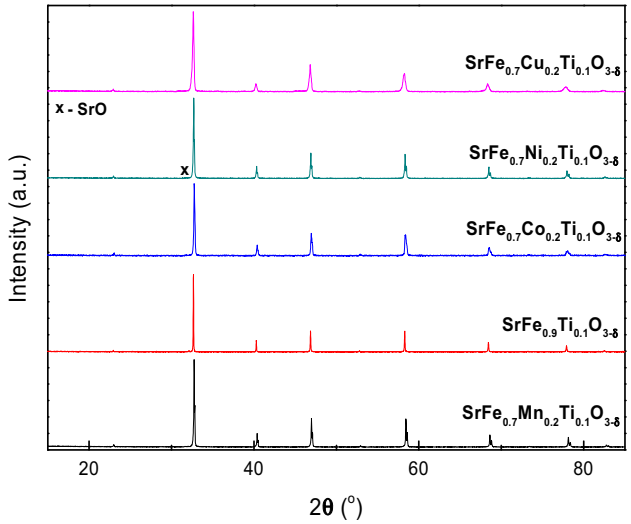

Fig. 1. X-ray diffraction pattern for $SrFe_{0.7}TM_{0.2}Ti_{0.1}O_{3-\delta}$ (TM = Mn, Fe, Co, Ni, Cu).

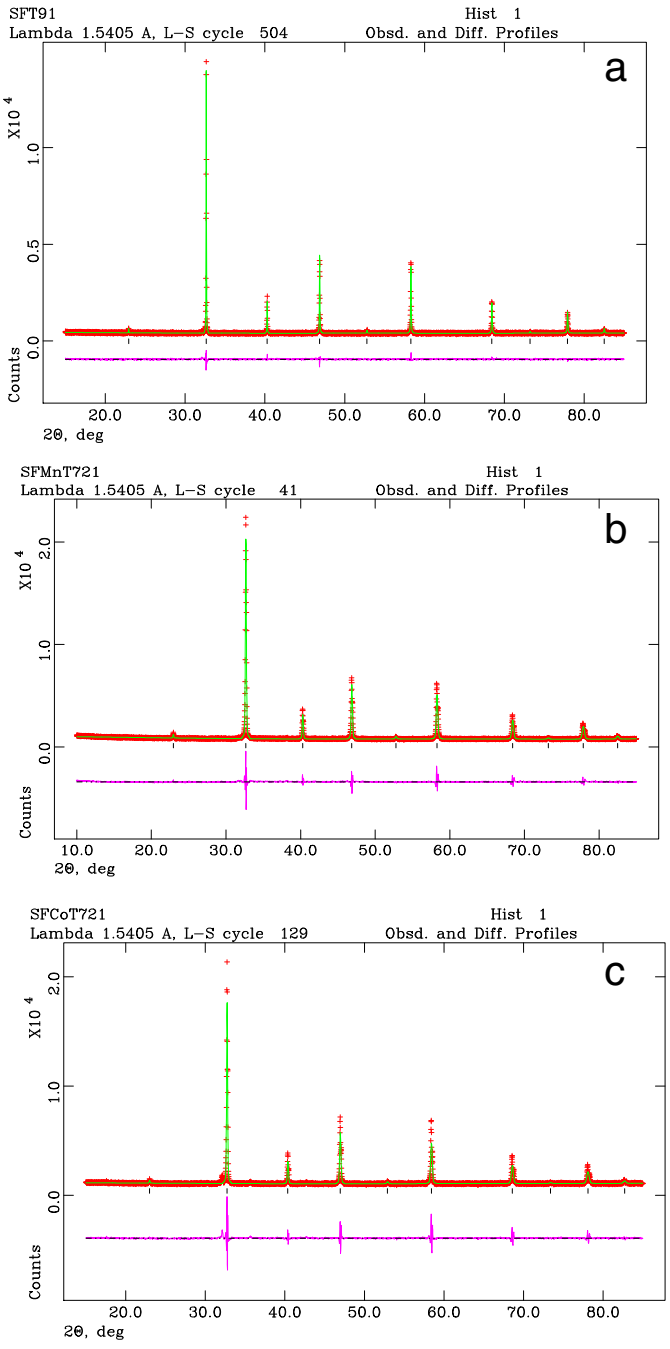

Fig. 2. Representative GSAS plots for $SrFe_{0.7}TM_{0.2}Ti_{0.1}O_{3-\delta}$ (TM = Fe (a), Mn (b), Co (c).

2.3. Conductivity testing

The pellets (ø ≈ 13 mm × 2 mm) were coated on opposing sides using silver paste and fired at 800 °C for 1 h to get rid of binders. The conductivity of the samples was measured in the range 300 °C to 700 °C, with the exception of $SrFe_{0.9}Ti_{0.1}O_{3-\delta}$ in 5% H_2/Ar which measured in the range 300 °C to 600 °C with a heating/cooling rate of 1 °C min^{-1}. Measurements in air and 5%H_2/Ar were conducted using an D.C. method by a pseudo-four-probe method using a Solartron 1287 electrochemical interface controlled by CorrWare software with a constant current of 0.01–0.1 A, as described in previous reports [24–26]. The temperature was digitally recorded in parallel with the impedance through an Omega HH506RA multi-logger thermometer connected to a

computer [26]. The conductivity in 5%H_2/Ar was measured after reduction the samples in the same atmosphere at 700 °C for 10 h.

3. Results and discussion

3.1. XRD and STA of $SrFe_{0.7}TM_{0.2}Ti_{0.1}O_{3-\delta}$ (TM = Mn, Fe, Co, Ni, Cu)

X-ray diffraction of $SrFe_{0.7}TM_{0.2}Ti_{0.1}O_{3-\delta}$ (TM = Mn, Fe, Co, Ni, Cu) after synthesis in air exhibited perovskite structures, space group *Pm-3m* (No. 221), for all compounds as shown in Fig. 1, albeit with a small amount, 3.5% phase fraction, of an SrO impurity phase (PDF: 6-520) observed for sample $SrFe_{0.7}Ni_{0.2}Ti_{0.1}O_{3-\delta}$. The representative GSAS plots for $SrFe_{0.7}TM_{0.2}Ti_{0.1}O_{3-\delta}$ with TM = Fe, Mn and Co are shown in Fig. 2. The refined lattice parameters are listed in Table 1. As shown in Fig. 3, a variation in the lattice parameters was exhibited which does not directly correlate with the variation in the average size of the dopant cations, with the lattice parameters reducing in the order Cu > Mn > Fe > Co > Ni. This is consistent to the trends of ionic radii for TM^{2+} ions at octahedral sites [27] although the real charge of TM ions in the. $SrFe_{0.7}TM_{0.2}Ti_{0.1}O_{3-\delta}$ series could be between TM^{2+} and TM^{4+}.

In previous reports, all dopants exhibited an reduction of the average oxidation state of iron in $SrFeO_{3-\delta}$ with increasing dopant concentration, with the larger cation size of Fe^{3+} over Fe^{4+} or the increase in the oxygen content resulting in an increase in the lattice parameters [17,28,29]. Due to the lower oxidation state of the dopants, it would be expected that a reduction in the lattice parameters, from Fe^{3+} to Fe^{4+} transitions and the reduction in oxygen content, would be observed with B^{2+} doping. This is true for both cobalt and nickel, which, due to the dopant sizes (0.745 Å for Co^{2+}_{oct}, 0.58 Å for Co^{2+}_{tet} and 0.69 Å for Ni^{2+}_{oct}, 0.55 Å for Ni^{2+}_{tet}), is indicative of Fe^{4+} formation. An increase in the lattice parameter with doping of copper (Cu^{2+}_{oct}, 0.73 Å) was observed, suggesting that the expansion resulting from Cu doping is higher than the lattice shrinkage from the Fe^{3+} to Fe^{4+} transition and the loss of oxygen from the structure, leading to lattice expansion. Doping of manganese elicits a minimal increase in the lattice parameter, 0.0019 Å, over $SrFe_{0.9}Ti_{0.1}O_{3-\delta}$, which, due to the size of the Mn^{2+} cation (0.83 Å for Mn^{2+}_{oct} or 0.66 Å for Mn^{2+}_{tet}), is either suggestive of Mn^{3+} formation (0.645 Å for Mn^{3+}_{oct} or 0.58 Å for Mn^{3+}_{tet}) or of preferential tetrahedral coordination, balancing the reduction from the Fe^{3+}-Fe^{4+} transition and the loss of oxygen from the structure. Further information on the oxidation state and coordination of the dopant cations or iron can only be obtained through additional analysis techniques, such as Mössbauer Spectroscopy or X-ray Photoelectron Spectroscopy (XPS).

Thermogravimetric analysis of $SrFe_{0.7}TM_{0.2}Ti_{0.1}O_{3-\delta}$ (TM = Mn, Fe, Co, Ni, Cu) in air are shown in Fig. 4a. The weight loss at low temperature is related to the loss of adsorbed water and gases and that at high temperature is related to loss of lattice oxygen. Samples $SrFe_{0.7}TM_{0.2}Ti_{0.1}O_{3-\delta}$ with TM = Fe, Co starts to lose oxygen at a temperature of ~450 °C whilst samples with TM = Mn, Cu starts to lose oxygen at ~500 °C indicating the latter is more stable in a reducing atmosphere. Sample $SrFe_{0.7}Ni_{0.2}Ti_{0.1}O_{3-\delta}$ kept losing weight during the whole process, possibly related to the presence of SrO impurity (Fig. 1). When stored at room temperature, the SrO may react with H_2O to form $Sr(OH)_2$ which will decompose on heating. Another possibility is that, sample $SrFe_{0.7}Ni_{0.2}Ti_{0.1}O_{3-\delta}$ tends to lose weight at lower temperature indicating it is the least stable one in the investigated oxides. Differential scanning calorimetry, Fig. 4b, reveals a reversible thermal effects for all compounds, observed between 600 °C and 700 °C on heating and between 750 °C and 700 °C on cooling. This could be related to the loss or lattice oxygen on heating and gain oxygen on cooling [8]. Phase transition is unlikely because the oxides already exhibit a highly symmetric cubic structure whilst high temperature phase transition in perovskite is normally from low to high symmetry at evaluated temperatures [30,31]. Further investigation is required.

3.2. Conductivity of $SrFe_{0.7}TM_{0.2}Ti_{0.1}O_{3-\delta}$ (TM = Mn, Fe, Co, Ni, Cu) in air

The conductivities of $SrFe_{0.7}TM_{0.2}Ti_{0.1}O_{3-\delta}$ (TM = Mn, Fe, Co, Ni, Cu) in air are shown in Fig. 5. Compared to $SrFe_{0.9}Ti_{0.1}O_{3-\delta}$, the conductivities increase for all transition metal dopants, with all compounds. In the $SrFe_{0.7}TM_{0.2}Ti_{0.1}O_{3-\delta}$ series, partially replacing iron by other transition elements Mn, Co, Ni and Cu leading to increased conductivity in air. It has been reported that the total electrical conductivity in $SrFe_{1-x}Co_xO_{3-\delta}$ increased when a large amount of cobalt was introduced in the solid solution [32]. Therefore it is also expected that sample $SrFe_{0.7}Co_{0.2}Ti_{0.1}O_{3-\delta}$ may exhibit high electrical conductivity than $SrFe_{0.9}Ti_{0.1}O_{3-\delta}$. As for elements Mn, Ni and Cu, they tend to exhibit lower state at high temperatures [33]. For charge balance, in samples co-doped with these elements, they can lose lattice oxygen to form more oxygen vacancies. This is likely to increase the oxygen ionic conductivity thus the total electrical conductivity increases as well. On the other hand, increase the charge of ion ions, say, more Fe^{n+} ions will exhibit the state of Fe^{4+} will lead to increased electronic conductivity [34]. The conductivity of $SrFe_{0.7}Mn_{0.2}Ti_{0.1}O_{3-\delta}$, $SrFe_{0.7}Co_{0.2}Ti_{0.1}O_{3-\delta}$ and $SrFe_{0.7}Cu_{0.2}Ti_{0.1}O_{3-\delta}$ remained between 5 S cm^{-1} and 20 S cm^{-1} over the measured temperature range, thus exhibiting potential for use as SOFC cathode materials. Previous research into $La_{0.8}Sr_{0.2}Co_{1-y}Fe_yO_{3-\delta}$ [35] suggests that the transition between semiconducting and metallic

Table 1
'Goodness of fit' parameters, lattice parameters and atomic parameters from GSAS refinement of $SrFe_{0.7}TM_{0.2}Ti_{0.1}O_{3-\delta}$ (TM = Mn, Fe, Co, Ni, Cu) after synthesis in air.

		$SrFe_{0.7}Mn_{0.2}Ti_{0.1}O_{3-\delta}$	$SrFe_{0.9}Ti_{0.1}O_{3-\delta}$	$SrFe_{0.7}Co_{0.2}Ti_{0.1}O_{3-\delta}$	$SrFe_{0.7}Ni_{0.2}Ti_{0.1}O_{3-\delta}$	$SrFe_{0.7}Cu_{0.2}Ti_{0.1}O_{3-\delta}$
χ^2		3.795	1.193	6.098	4.086	3.038
Rp (%)		6.40	5.21	7.15	9.75	5.64
wRp (%)		4.56	4.11	4.41	6.89	4.11
Space group		*Pm-3m*	*Pm-3m*	*Pm-3m*	*Pm-3m*	*Pm-3m*
a (Å)		3.8759(2)	3.8740(2)	3.8673(1)	3.8551(10)	3.8833(1)
V (Å^3)		58.22(1)	58.14(1)	57.84(1)	57.29(4)	58.56(3)
Sr	x	0	0	0	0	0
	y	0	0	0	0	0
	z	0	0	0	0	0
	U_{iso}	0.009(7)	0.004(3)	0.007(1)	0.003(1)	0.012(1)
Fe/TM/Ti	x	0.5	0.5	0.5	0.5	0.5
	y	0.5	0.5	0.5	0.5	0.5
	z	0.5	0.5	0.5	0.5	0.5
	U_{iso}	0.013(1)	0.006(6)	0.007(1)	0.001(1)	0.002(1)
O	x	0	0	0	0	0
	y	0.5	0.5	0.5	0.5	0.5
	z	0.5	0.5	0.5	0.5	0.5
	U_{iso}	0.032(1)	0.022(1)	0.027(5)	0.016(3)	0.025(1)

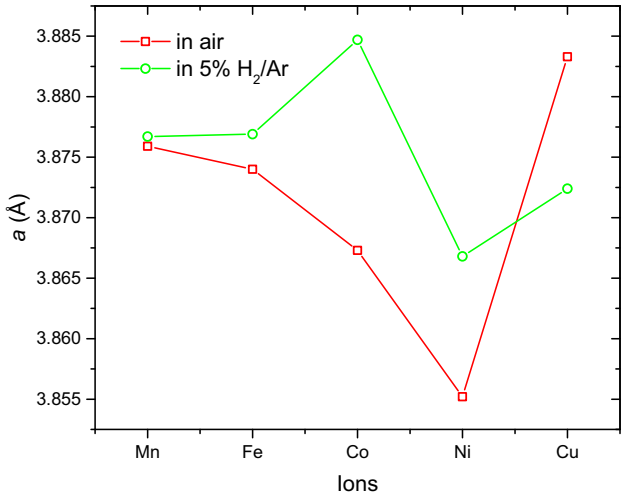

Fig. 3. Variation of lattice parameters for $SrFe_{0.7}TM_{0.2}Ti_{0.1}O_{3-\delta}$ (TM = Mn, Fe, Co, Ni, Cu) samples prepared in air and after reduction in 5%H_2/Ar at 700 °C for 10 h.

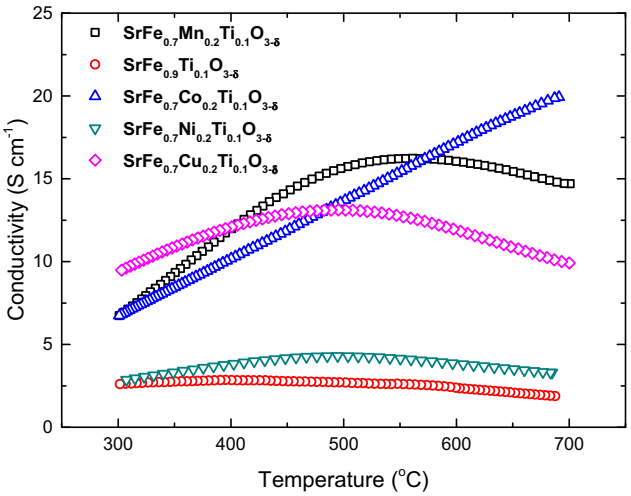

Fig. 5. Conductivity of $SrFe_{0.7}TM_{0.2}Ti_{0.1}O_{3-\delta}$ (TM = Mn, Fe, Co, Ni, Cu) in air.

behaviour would still be observed for cobalt doped ferrites; however, the transition for $La_{0.8}Sr_{0.2}Co_{1-y}Fe_yO_{3-\delta}$ occurs as higher temperatures than the measurement temperature range used in this study. In our study, it is difficult to obtain pellets with higher relative density by conventional sintering method because the pellets melt at higher sintering temperature. The relatively low relative density may affect the measured conductivity because of the existence of void in the pellets. In general, the measured conductivity is lower than the specific conductivity (conductivity of a fully dense sample) [36–39]. In reported materials, difference between the measured apparent conductivity and specific conductivity is generally not big when the relative density is higher than 70% [37,39]. As the density of our samples is over 70%, the measured conductivity is lower than specific conductivity but should be fairly close.

3.3. STA and conductivity of $SrFe_{0.7}TM_{0.2}Ti_{0.1}O_{3-\delta}$ (TM = Mn, Fe, Co, Ni, Cu) in 5%H_2/Ar

Reduction of $SrFe_{0.7}TM_{0.2}Ti_{0.1}O_{3-\delta}$ (TM = Mn Ni, Cu) at 700 °C in 5% H_2/Ar exhibited a lower weight loss than was observed for $SrFe_{0.9}Ti_{0.1}O_{3-\delta}$ (Fig. 6). In contrast to the other doped compounds, $SrFe_{0.7}Co_{0.2}Ti_{0.1}O_{3-\delta}$ exhibited an increase in weight loss, 6.4%, compared to that for $SrFe_{0.9}Ti_{0.1}O_{3-\delta}$, 5.05%. The increased weight loss is likely indicative of reduction of cobalt at these temperatures. In general, in the presence of hydrogen, the oxides tend to lose weight at lower temperatures compared to those in air (Fig. 4).

The conductivities of the transition metal doped samples reduced at 700 °C in 5% H_2/Ar are shown in Fig. 7. The samples exhibited minor reductions in the conductivity, with the exception of the manganese

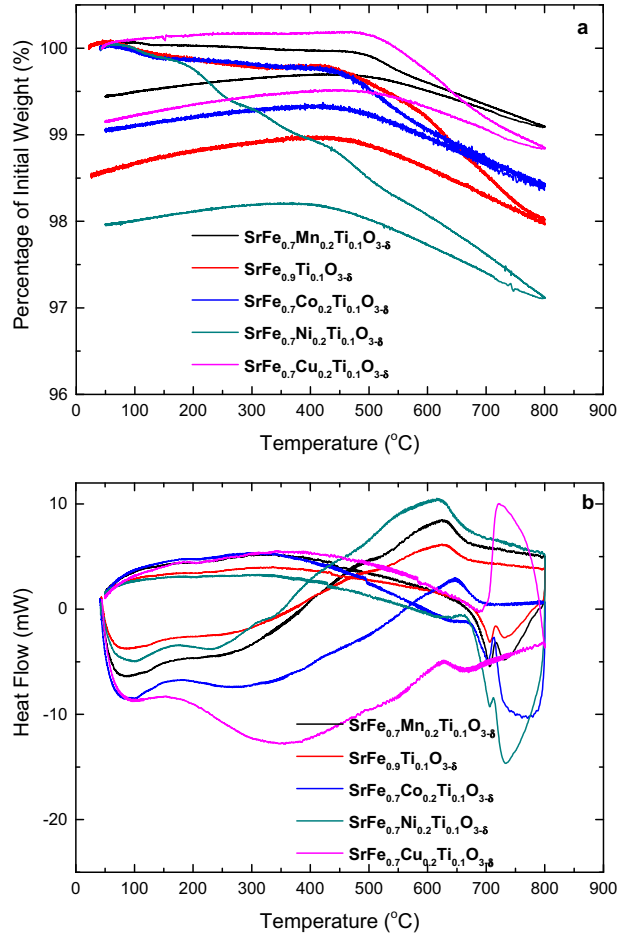

Fig. 4. Thermogravimetric analysis (a) and differential scanning calorimetry (b) of $SrFe_{0.7}TM_{0.2}Ti_{0.1}O_{3-\delta}$ (TM = Mn, Fe, Co, Ni, Cu) in air.

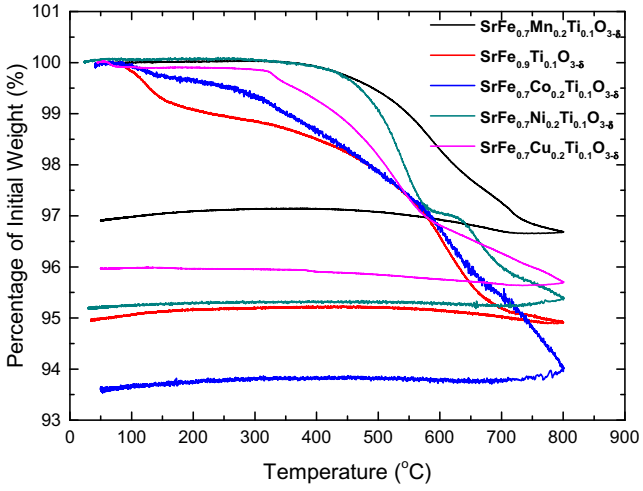

Fig. 6. Thermogravimetric analysis of $SrFe_{0.7}TM_{0.2}Ti_{0.1}O_{3-\delta}$ (TM = Mn, Fe, Co, Ni, Cu) in 5% H_2/Ar.

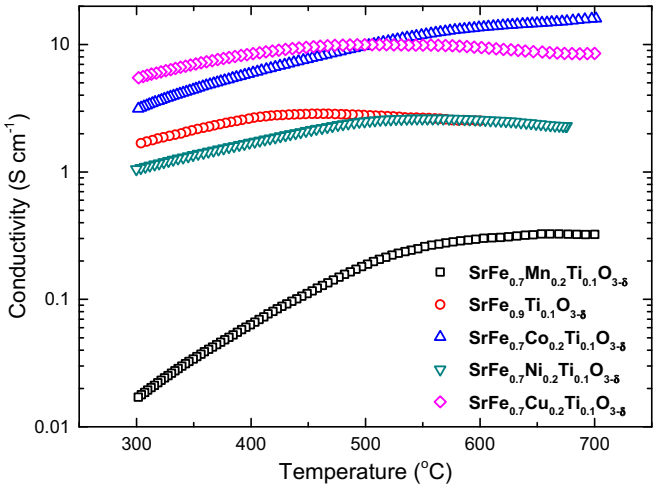

Fig. 7. Conductivity of $SrFe_{0.7}TM_{0.2}Ti_{0.1}O_{3-\delta}$ (TM = Mn, Fe, Co, Ni, Cu) in 5% H_2/Ar.

doped sample. Minimal reduction of the conductivity of $SrFe_{0.7}Co_{0.2}Ti_{0.1}O_{3-\delta}$, $SrFe_{0.7}Ni_{0.2}Ti_{0.1}O_{3-\delta}$ and $SrFe_{0.7}Cu_{0.2}Ti_{0.1}O_{3-\delta}$ is suggestive of minor decreases in the charge carrier concentration at these temperatures. This correlates with the minor decrease in the activation energy, 0.02–0.07 eV, noted for the cobalt, nickel and copper doped compounds upon reduction.

The conductivity of the Mn doped sample demonstrated a reduction of several orders of magnitude, 14.69 S cm^{-1} in air to 0.323 S cm^{-1} in 5% H_2/Ar at 700 °C. This was also demonstrated in the increase in the activation energy upon reduction, from 0.226(1) eV to 0.516(1) eV. The semiconductor-metal transition observed in air is also exhibited, albeit at higher temperature, from 560 °C to 660 °C upon reduction, suggesting that the conduction mechanism does not change. The reduction in conductivity is likely associated with a significant decrease in the charge carrier concentration, as a result of cationic reduction. This may intimate that manganese dopes as Mn^{3+}, directly contributing to the charge carrier concentration in air, and not altering the charge carrier concentration through charge compensation mechanisms. Reduction of Mn^{3+} to Mn^{2+} upon exposure to 5% H_2/Ar would reduce the charge carrier concentration, similar to the Fe^{4+}-Fe^{3+} transition. Significant reductions in the electronic conductivity is also observed for manganite perovskites, as a result of Mn^{3+}-Mn^{2+} transitions [40]. It should be noted that the

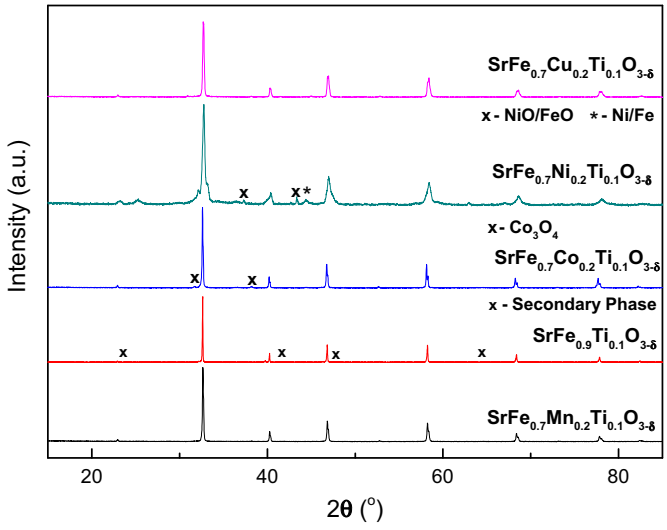

Fig. 8. X-ray diffraction pattern of $SrFe_{0.7}TM_{0.2}Ti_{0.1}O_{3-\delta}$ (TM = Mn, Fe, Co, Ni, Cu) after reduction in 5% H_2/Ar at 700 °C.

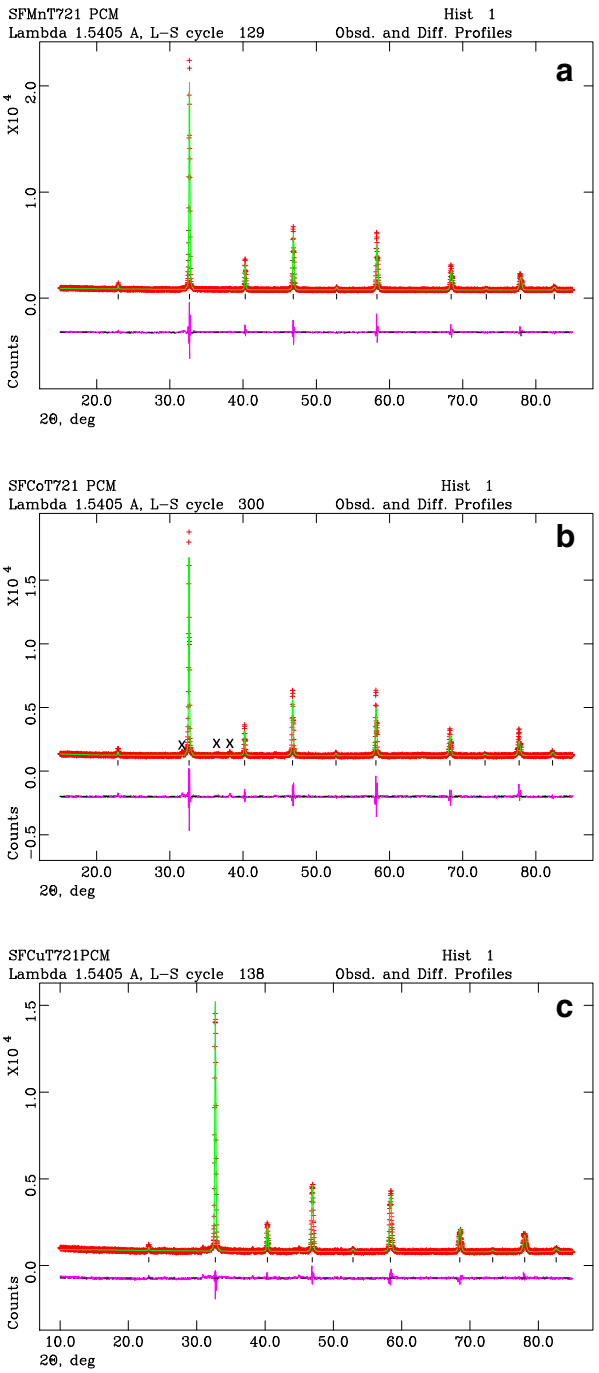

Fig. 9. Representative GSAS plots for $SrFe_{0.7}TM_{0.2}Ti_{0.1}O_{3-\delta}$ (TM = Mn (a), Co (b), Cu (c) after reduction in 5%H_2/Ar at 700 °C. x: Co_3O_4.

specific conductivities of the samples in a reducing atmosphere are expected higher than the measured apparent conductivity, as described above. Low relative density will not affect the application of these materials as electrode for solid oxide fuel cells or solid oxide electrolytic cells as the electrodes have to be porous to allow gas diffusion to the triple phase boundary to realize the electrochemical reactions on the electrodes [41–44].

3.4. XRD of reduced $SrFe_{0.7}TM_{0.2}Ti_{0.1}O_{3-\delta}$ (TM = Mn, Fe, Co, Ni, Cu)

X-ray diffraction of $SrFe_{0.7}TM_{0.2}Ti_{0.1}O_{3-\delta}$ (TM = Mn, Fe, Co, Ni, Cu) after reduction at 700 °C in 5% H_2/Ar are shown in Fig. 8. Little change in the material structure, with the exception of $SrFe_{0.7}Ni_{0.2}Ti_{0.1}O_{3-\delta}$

Table 2
'Goodness of fit' parameters, lattice parameters and atomic parameters from GSAS refinement of $SrFe_{0.7}TM_{0.2}Ti_{0.1}O_{3-\delta}$ (TM = Mn, Fe, Co, Ni, Cu) after reduction at 700 °C in 5% H_2/Ar.

		$SrFe_{0.7}Mn_{0.2}Ti_{0.1}O_{3-\delta}$	$SrFe_{0.9}Ti_{0.1}O_{3-\delta}$	$SrFe_{0.7}Co_{0.2}Ti_{0.1}O_{3-\delta}$	$SrFe_{0.7}Ni_{0.2}Ti_{0.1}O_{3-\delta}$	$SrFe_{0.7}Cu_{0.2}Ti_{0.1}O_{3-\delta}$
χ^2		4.275	1.657	4.896	4.665	2.490
Rp (%)		6.79	6.44	6.06	6.43	5.15
wRp (%)		4.66	4.91	3.73	4.85	3.94
Space group		*Pm-3m*	*Pm-3m*	*Pm-3m*	*Pm-3m*	*Pm-3m*
a (Å)		3.8767(2)	3.8769(2)	3.8847(1)	3.8759(7)	3.8724(7)
V (Å^3)		58.26(1)	58.27(1)	58.62(1)	58.22(2)	58.07(3)
Sr	x	0	0	0	0	0
	y	0	0	0	0	0
	z	0	0	0	0	0
	U_{iso}	0.009(1)	0.005(1)	0.002(1)	0.020(1)	0.003(6)
Fe/TM/Ti	x	0.5	0.5	0.5	0.5	0.5
	y	0.5	0.5	0.5	0.5	0.5
	z	0.5	0.5	0.5	0.5	0.5
	U_{iso}	0.011(10)	0.007(9)	0.004(1)	0.004(2)	0.004(9)
O	x	0	0	0	0	0
	y	0.5	0.5	0.5	0.5	0.5
	z	0.5	0.5	0.5	0.5	0.5
	U_{iso}	0.031(1)	0.028(1)	0.026(2)	0.034(3)	0.036(1)

which exhibits a 5.6% phase fraction of NiO (PDF: 4-835) and a 4.4% phase fraction of Ni (PDF: 6-696) and $SrFe_{0.9}Ti_{0.1}O_{3-\delta}$ which exhibits an unidentified impurity phase. A small amount of Co_3O_4 (PDF: 80–1545) second phase was also observed in the reduced $SrFe_{0.7}Co_{0.2}Ti_{0.1}O_{3-\delta}$ [45,46]. The redox instability observed for the nickel and cobalt doped phase is likely due to the reducibility of the nickel and cobalt within the structure, further implied by exsolution of nickel metal. This has also been observed for other nickel or cobalt doped perovskite materials [47–49].

GSAS [23] analysis of these compounds exhibits an increase in the lattice parameters for $SrFe_{0.9}Ti_{0.1}O_{3-\delta}$, $SrFe_{0.7}Co_{0.2}Ti_{0.1}O_{3-\delta}$ and $SrFe_{0.7}Ni_{0.2}Ti_{0.1}O_{3-\delta}$ upon reduction. Fig. 9 shows the representative GSAS plots for $SrFe_{0.7}TM_{0.2}Ti_{0.1}O_{3-\delta}$ (TM = Mn, Co and Cu) after reduction in 5%H_2/Ar at 700 °C. The refinced lattice parameters are listed in Table 2 and plotted in Fig. 3, which is indicative of partial reduction of the B-site cations. Compared to the lattice parameters for the oxides in air (Fig. 3). The largest lattice parameter change was observed for sample $SrFe_{0.7}Co_{0.2}Ti_{0.1}O_{3-\delta}$, increased from 3.8673(1) to 3.8847(1) Å which is probably due to the reduction of cobalt and segregation of Co_3O_4 in a reducing atmosphere. Sample $SrFe_{0.7}Co_{0.2}Ti_{0.1}O_{3-\delta}$ also exhibited the largest weight loss on STA analysis in 5%H_2/Ar (Fig. 6). Whilst reduction would be expected to result in an increase in the lattice parameter, a minor reduction in the lattice parameter of $SrFe_{0.7}Cu_{0.2}Ti_{0.1}O_{3-\delta}$ was observed. This is likely a result of the lattice shrinkage from oxygen loss and possible changes in the cationic coordination environment, overcoming the lattice expansion from cationic reduction.

In contrast to other dopants, sample $SrFe_{0.7}Mn_{0.2}Ti_{0.1}O_{3-\delta}$ exhibits almost no change in the lattice parameters after reduction at 700 °C. Whilst this would normally suggest minimal variation in the material properties, a significant variation in the conductivity is observed upon reduction. Cationic reduction is known to occur and therefore would be expected to induce lattice expansion. In this case a balance between lattice shrinkage and lattice expansion is posited to occur, resulting in the stability of the lattice parameter upon reduction.

An improvement in the stability and conductivity in both air and 5% H_2/Ar of $SrFe_{0.9}Ti_{0.1}O_{3-\delta}$ was achieved through doping of copper and manganese, forming $SrFe_{0.7}Cu_{0.2}Ti_{0.1}O_{3-\delta}$ and $SrFe_{0.7}Mn_{0.2}Ti_{0.1}O_{3-\delta}$. However, the observed conductivity of $SrFe_{0.7}Mn_{0.2}Ti_{0.1}O_{3-\delta}$ in a reducing atmosphere is below 0.4 S cm^{-1} at a temperature below 700 °C (Fig. 7) which is insufficient to be a good anode for SOFCs. It has been reported that doping of Mn at the B-site of $SrFe_{0.75}Mo_{0.25}O3$-δ led to reduced conductivity in reducing atmospheres [13]. As $SrFe_{0.7}Cu_{0.2}Ti_{0.1}O_{3-\delta}$ exhibits high electrical conductivity in both air and 5%H_2/Ar, it is potential electrode materials for reversible and symmetrical solid oxide fuel cells [9,10,13,14]. Whilst manganese doping improved the redox stability and conductivity in air, the reduction of the conductivity in 5% H_2/Ar renders this compound unsuitable for use as an anode material for SOFCs. Nickel doping achieved only a minimal increase in conductivity in both air and 5% H_2/Ar. Although $SrFe_{0.7}Co_{0.2}Ti_{0.1}O_{3-\delta}$ exhibits high conductivity in a reducing atmosphere but it did not exhibit redox stability thus is not suitable for use as an SOFC electrode material at a temperature close to 700 °C. However, the stability of an oxide in a reducing atmosphere is related to the temperature. It might be stable at lower temperature thus still can be used as redox stable anode for fuel cells operating at reduced temperature, say, around 500 °C. Further investigation is required to confirm this.

4. Conclusions

The cubic perovskite structure was observed for all dopants for $SrFe_{0.7}TM_{0.2}Ti_{0.1}O_{3-\delta}$ (TM = Mn, Fe, Co, Ni, Cu), with variation in the lattice parameters associated with different dopant environments and charge compensation mechanisms. Improvement of the electronic conductivity over $SrFe_{0.9}Ti_{0.1}O_{3-\delta}$ was observed for all dopants in air, attributed to increasing charge carrier concentration. Reduction in 5% H_2/Ar exhibited minimal variation in material properties $SrFe_{0.7}Cu_{0.2}Ti_{0.1}O_{3-\delta}$, with a significant reduction in conductivity was observed for $SrFe_{0.7}Mn_{0.2}Ti_{0.1}O_{3-\delta}$. A small amount of SrO was observed in sample with nominal composition $SrFe_{0.7}Ni_{0.2}Ti_{0.1}O_{3-\delta}$. All doped compounds exhibited a single phase cubic perovskite structure after reduction with the exception of $SrFe_{0.7}Ni_{0.2}Ti_{0.1}O_{3-\delta}$ and $SrFe_{0.7}Co_{0.2}Ti_{0.1}O_{3-\delta}$ which display secondary nickel and cobalt phases respectively upon reduction.

The significant improvement in the conductivity and stability upon doping of $SrFe_{0.9}Ti_{0.1}O_{3-\delta}$ suggests that a more suitable parent compound may produce further improvements in material conductivity and stability. $SrFe_{0.7}Cu_{0.2}Ti_{0.1}O_{3-\delta}$ are redox stable at a temperature below 700 °C and highly conductive with conductivities around 10 S cm^{-1} in both air and reducing atmosphere which are about five times higher than those of pure $SrFe_{0.9}Ti_{0.1}O_{3-\delta}$. In the investigated oxides, in terms of conductivity and redox stability, $SrFe_{0.7}Cu_{0.2}Ti_{0.1}O_{3-\delta}$ exhibits promising properties for use as a potential electrode material for symmetrical/reversible SOFCs.

Acknowledgements

The authors thank EPSRC Flame SOFCs (EP/K021036/2), UK-India Biogas SOFCs (EP/I037016/1) and SuperGen Fuel Cells (EP/G030995/1)

projects for funding. We also thank Natural Science Foundation of China (NSFC21628301) for support. One of the authors (Cowin) thanks ScotChem SPIRIT scheme for support of his PhD study.

References

[1] P.I. Cowin, C.T.G. Petit, R. Lan, J.T.S. Irvine, S.W. Tao, Adv. Energy Mater. 1 (2011) 314.
[2] X.-M. Ge, S.-H. Chan, Q.-L. Liu, Q. Sun, Adv. Energy Mater. 2 (2012) 1156.
[3] S. Sengodan, S. Choi, A. Jun, T.H. Shin, Y.-W. Ju, H.Y. Jeong, J. Shin, J.T.S. Irvine, G. Kim, Nat. Mater. 14 (2015) 205.
[4] S.W. Tao, J.T.S. Irvine, Nat. Mater. 2 (2003) 320.
[5] Y.H. Huang, R.I. Dass, Z.L. Xing, J.B. Goodenough, Science 312 (2006) 254.
[6] J.C. Ruiz-Morales, J. Canales-Vazquez, C. Savaniu, D. Marrero-Lopez, W.Z. Zhou, J.T.S. Irvine, Nature 439 (2006) 568.
[7] C.H. Yang, Z.B. Yang, C. Jin, G.L. Xiao, F.L. Chen, M.F. Han, Adv. Mater. 24 (2012) 1439.
[8] R. Lan, P.I. Cowin, S. Sengodan, S.W. Tao, Sci. Report. 6 (2016) 31839.
[9] D.M. Bastidas, S.W. Tao, J.T.S. Irvine, J. Mater. Chem. 16 (2006) 1603.
[10] J.C. Ruiz-Morales, D. Marrero-Lopez, J. Canales-Vazquez, J.T.S. Irvine, RSC Adv. 1 (2011) 1403.
[11] O.A. Marina, L.R. Pederson, M.C. Williams, G.W. Coffey, K.D. Meinhardt, C.D. Nguyen, E.C. Thomsen, J. Electrochem. Soc. 154 (2007) B452.
[12] P.I. Cowin, R. Lan, C.T.G. Petit, H. Wang, S. Tao, J. Mater. Sci. 51 (2016) 4115.
[13] K. Zheng, K. Swierczek, J.M. Polfus, M.F. Sunding, M. Pishahang, T. Norby, J. Electrochem. Soc. 162 (2015) F1078.
[14] Q. Liu, X.H. Dong, G.L. Xiao, F. Zhao, F.L. Chen, Adv. Mater. 22 (2010) 5478.
[15] S. Cho, D.E. Fowler, E.C. Miller, J.S. Cronin, K.R. Poeppelmeier, S.A. Barnett, Energy Environ. Sci. 6 (2013) 1850.
[16] J.C. Waerenborgh, D.P. Rojas, A.L. Shaula, G.C. Mather, M.V. Patrakeev, V.V. Kharton, J.R. Frade, Mater. Lett. 59 (2005) 1644.
[17] M.V. Patrakeev, V.V. Kharton, Y.A. Bakhteeva, A.L. Shaula, I.A. Leonidov, V.L. Kozhevnikov, E.N. Naumovich, A.A. Yaremchenko, F.M.B. Marques, Solid State Sci. 8 (2006) 476.
[18] M.V. Patrakeev, A.A. Markov, I.A. Leonidov, V.L. Kozhevnikov, V.V. Kharton, Solid State Ionics 177 (2006) 1757.
[19] P.I. Cowin, R. Lan, C.T.G. Petit, S.W. Tao, Solid State Sci. 46 (2015) 62.
[20] G. Yang, C. Su, Y. Chen, F. Dong, M.O. Tade, Z. Shao, J. Eur. Ceram. Soc. 35 (2015) 2531.
[21] L. dos Santos-Gomez, J.M. Porras-Vazquez, E.R. Losilla, D. Marrero-Lopez, RSC Adv. 5 (2015) 107889.
[22] S. Jiang, J. Sunarso, W. Zhou, J. Shen, R. Ran, Z. Shao, J. Power Sources 298 (2015) 209.
[23] A.C. Larson, R.B.V. Dreele, General structural analysis system, Los Alamos National Laboratory Report LAUR, 86, 1994.
[24] P.I. Cowin, R. Lan, C.T. Petit, L. Zhang, S.W. Tao, J. Alloys Compd. 509 (2011) 4117.
[25] P.I. Cowin, R. Lan, L. Zhang, C.T.G. Petit, A. Kraft, S.W. Tao, Mater. Chem. Phys. 126 (2011) 614.
[26] C.T.G. Petit, R. Lan, P.I. Cowin, J.T.S. Irvine, S.W. Tao, J. Mater. Chem. 21 (2011) 525.
[27] R.D. Shannon, Acta Crystallogr. A 32 (1976) 751.
[28] G. Xiao, Q. Liu, S. Wang, V.G. Komvokis, M.D. Amiridis, A. Heyden, S. Ma, F. Chen, J. Power Sources 202 (2012) 63.
[29] Y. Takeda, K. Kanno, T. Takada, O. Yamamoto, M. Takano, N. Nakayama, Y. Bando, J. Solid State Chem. 63 (1986) 237.
[30] I. Levin, J.Y. Chan, R.G. Geyer, J.E. Maslar, T.A. Vanderah, J. Solid State Chem. 156 (2001) 122.
[31] S.W. Tao, J.T.S. Irvine, Chem. Mater. 18 (2006) 5453.
[32] K. Wiik, S. Aasland, H.L. Hansen, I.L. Tangen, R. Odegard, Solid State Ionics 152 (2002) 675.
[33] T. Nakamura, G. Petzow, L.J. Gauckler, Mater. Res. Bull. 14 (1979) 649.
[34] S.W. Tao, J. Canales-Vázquez, J.T.S. Irvine, Chem. Mater. 16 (2004) 2309.
[35] L.W. Tai, M.M. Nasrallah, H.U. Anderson, D.M. Sparlin, S.R. Sehlin, Solid State Ionics 76 (1995) 259.
[36] J. Mizusaki, S. Tsuchiya, K. Waragai, H. Tagawa, Y. Arai, Y. Kuwayama, J. Am. Ceram. Soc. 79 (1996) 109.
[37] M. Marinsek, Materiali in Tehnologije 43 (2009) 79.
[38] D. Perez-Coll, E. Sanchez-Lopez, G.C. Mather, Solid State Ionics 181 (2010) 1033.
[39] P.J. Panteix, I. Julien, P. Abelard, D. Bernache-Assollant, Ceram. Int. 34 (2008) 1579.
[40] E.O. Ahlgren, F.W. Poulsen, Solid State Ionics 86–88 (1996) 1173.
[41] A. Atkinson, S. Barnett, R.J. Gorte, J.T.S. Irvine, A.J. McEvoy, M. Mogensen, S.C. Singhal, J. Vohs, Nat. Mater. 3 (2004) 17.
[42] S.W. Tao, J.T.S. Irvine, Chem. Rec. 4 (2004) 83.
[43] S.W. Tao, Q.Y. Wu, D.K. Peng, G.Y. Meng, J. Appl. Electrochem. 30 (2000) 153.
[44] B.C.H. Steele, A. Heinzel, Nature 414 (2001) 345.
[45] K.S. Kim, Y.J. Park, Nanoscale Res. Lett. 7 (2012) 47.
[46] R. Lan, S.W. Tao, ChemElectroChem 1 (2014) 2098.
[47] W. Kobsiriphat, B.D. Madsen, Y. Wang, M. Shah, L.D. Marks, S.A. Barnett, J. Electrochem. Soc. 157 (2010) B279.
[48] W. Bao, H. Guan, J. Cheng, J. Power Sources 175 (2008) 232.
[49] L.Z. Gan, L.T. Ye, S.W. Tao, K. Xie, Phys. Chem. Chem. Phys. 18 (2016) 3137.